

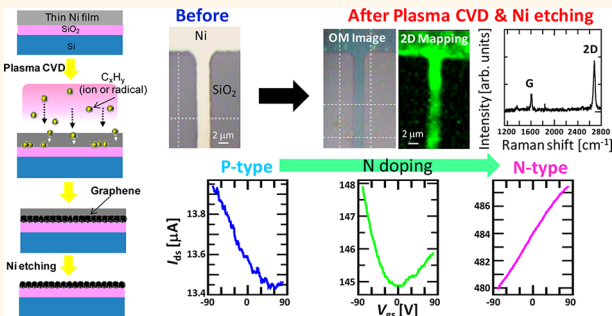
Direct Growth of Doping-Density-Controlled Hexagonal Graphene on SiO₂ Substrate by Rapid-Heating Plasma CVD

Toshiaki Kato* and Rikizo Hatakeyama

Department of Electronic Engineering, Tohoku University, Aoba 6-6-05, Aramaki-Aza, Aoba-Ku, Sendai 980-8579, Japan

Graphene is a monolayer carbon sheet possessing high carrier mobility, flexibility, and high optical transmittance.^{1–3} These properties are advantageous if graphene is to be used as a component in electrical devices such as field effect transistors,⁴ solar cells,⁵ and various gas⁶ and chemical⁷ sensors. Chemical vapor deposition (CVD) is one of the most promising methods of growing graphene, which can produce large and relatively high-quality graphene sheets.^{8–11} A graphene layer on an insulating layer, especially on an insulating SiO₂ substrate, is an important structural arrangement used in the fabrication of graphene-based electrical devices. Currently, graphene layers on SiO₂ substrates are fabricated by the following process. First, graphene is grown on Ni,^{8,9} Cu,¹⁰ or Co¹¹ surfaces (foil or deposited films on a substrate). These metal surfaces are necessary for the growth of graphene, as they decompose hydrocarbon gases and promote the nucleation of graphene. The graphene layer is then transferred to a SiO₂ substrate using polymer capping and chemical etching techniques.⁸ This process can fabricate relatively large-scale graphene sheets on an insulating substrate. However, it is difficult to transfer specific and fine graphene structures, such as graphene nanoribbons¹² or nanoscale patterned graphene, to specific points on a device. This precise placement of graphene is important when fabricating many widely used silicon-based electrical devices. The direct growth of graphene on an insulating substrate is an alternative approach to the above method. It is a challenging method, however, and only a few studies about the direct growth approach have so far been reported.^{13,14} The direct growth of multilayer nanographene using catalyst-free plasma CVD over a long period of time was reported.¹³ The growth of single-layer graphene over a small area of an insulating

ABSTRACT



A transfer-free method for growing carrier-density-controlled graphene directly on a SiO₂ substrate has been realized for the first time by rapid-heating plasma chemical vapor deposition (RH-PCVD). Using this method, high-quality single-layer graphene sheets with a hexagonal domain can be selectively grown between a Ni film and a SiO₂ substrate. Systematic investigations reveal that the relatively thin Ni layer, rapid heating, and plasma CVD are critical to the success of this unique method of graphene growth. By applying this technique, an easy and scalable graphene-based field effect transistor (FET) fabrication is also demonstrated. The electrical transport type of the graphene-based FET can be precisely tuned by adjusting the NH₃ gas concentration during the RH-PCVD process.

KEYWORDS: graphene sheet · direct growth · plasma CVD · carrier doping

substrate was also demonstrated by dewetting and evaporating Cu layers with an extended annealing time in the thermal CVD process.¹⁴ However, several critical issues relating to the yield, layer number control, large-scale growth, and tunable carrier doping are still to be resolved before the direct growth method is suitable for industrial processes to generate graphene-based electronics.

Here we report a novel, simple, and scalable method for the direct growth of graphene on an insulating substrate with tunable carrier doping. It is revealed that by adjusting the growth parameters using rapid-heating plasma chemical vapor deposition (RH-PCVD), the graphene layer can be made to grow along the interface

* Address correspondence to kato12@eiei.tohoku.ac.jp.

Received for review November 5, 2011
and accepted September 4, 2012.

Published online September 12, 2012
10.1021/nn302290z

© 2012 American Chemical Society

of the Ni layer and the SiO_2 substrate instead of on top of the Ni layer. The direct fabrication method is completed by removing the Ni layer using a chemical etching process, leaving large-area and high-quality single-layer graphene sheets on a SiO_2 substrate. Since the plasma process is used in this method, it can lower the growth temperature below 600 °C, which is much lower than the temperatures needed for thermal CVD graphene growth (900–1000 °C).^{8–11} Furthermore, an easy method for fabricating graphene-based field effect transistors (FET) is developed by applying this RH-PCVD direct growth method for graphene. The charge neutral point of the graphene-based FET can be shifted from the positive to the negative gate bias regions by controlling the NH_3 gas concentration during the RH-PCVD process. After completing this study, we became aware of a recently published study describing a similar method.¹⁵ In that study, a Cu catalytic layer with thermal CVD (~900 °C) was used, and graphene sheets were grown both on top of the Cu film and along the interface between the Cu and SiO_2 layers. This differs from our method, where a Ni catalytic layer and RH-PCVD (~600 °C) were used, and graphene sheets are grown only along the interface of the Ni and SiO_2 layers. Because graphene sheets are not formed on top of the Ni layer in our method, the Ni films are easily removed using a chemical etching technique without requiring any extra ashing process.¹⁵ Furthermore, in this recently reported study, the graphene directly fabricated on the SiO_2 substrate was highly p-doped due to the strong interaction between graphene and SiO_2 .¹⁵ In contrast, our method demonstrates a transport-type tuning of the doping of directly grown graphene for the first time. This is significant for the construction of graphene-based electrical devices, such as logic circuits, which typically require spatially varying dopant concentrations within a single graphene layer.

RESULTS AND DISCUSSION

Figure 1 illustrates the basic concept of our approach for growing graphene directly on an insulating substrate. A Ni film was deposited on a SiO_2 (300 nm)/Si by vacuum evaporation (Figure 1a). The graphene growth was realized using a homemade plasma CVD system with a mixture of methane and hydrogen gas. The substrate was immediately transferred from outside the electrical furnace to the furnace center, and the substrate temperature increased to the required temperature for growth (typically 600–975 °C) within 1 min. After heating the substrate, radio frequency power (rf; 13.56 MHz) was supplied to the coils outside of a quartz tube to generate a plasma (Figure 1b). The substrate temperature was immediately decreased after completing the plasma CVD process (Figure 1c). During the cooling process, the graphene layer could be preferentially grown along the interface between

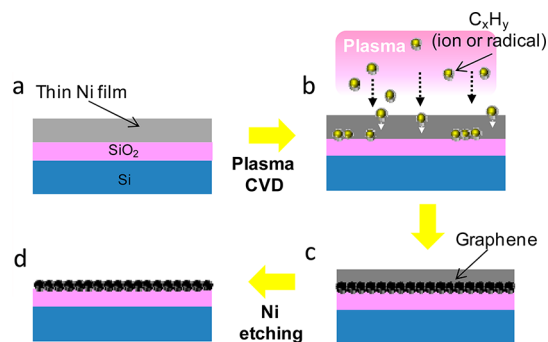


Figure 1. Schematic illustration of the basic approach for our method for the direct growth of graphene on a SiO_2 surface. (a) A thin Ni film is deposited on a SiO_2 /Si substrate. (b) Plasma CVD is performed. (c) Carbon atoms diffuse in the Ni film, and graphene is preferentially grown along the interface between the Ni and SiO_2 layers. (d) Graphene on a SiO_2 /Si substrate is realized by removing the Ni film using a chemical etching technique.

the Ni film and SiO_2 substrate. Finally, the deposited Ni film was removed using a conventional chemical etching technique with FeCl_3 or HCl solution (Figure 1d).

Scanning electron microscope (SEM) observations and Raman mapping measurements were carried out for the fabricated materials *before* the Ni film was removed. The detailed growth conditions are as follows: methane to hydrogen mixture ratio of 9:1; substrate temperature, T_{sub} , of 950 °C; growth time, t_g , of 30 s; radio frequency power, P_{rf} , of 110 W; and a Ni film thickness, T_{Ni} , of 55 nm. Hole-like structures were observed over the entire surface of the Ni film (Figure 2a). Figure 2b shows an optical microscope image of the Ni film surface. Integrated Raman intensity maps of the Si-peak (512 – 540 cm^{-1}), the G-peak (1544 – 1626 cm^{-1}), and the 2D-peak (2577 – 2700 cm^{-1}) are shown in Figure 2c, d, and e, respectively. The intensity ratio of the 2D-peak to the G-peak is shown in Figure 2f. It should be noted that Figure 2b–f are shown at the same scale and position. Because the strong Si-peak appears only at the hole-like structures, the Ni film should be partially evaporated and the SiO_2 surface appears at the hole-like structures (Figure 2c). The G-peak and 2D-peak are detected only at the hole-like structures (Figure 2d and e), and the intensity of the 2D-peak is much higher than that of the G-peak at the hole-like structures (Figure 2f). This is also confirmed with the raw Raman scattering spectra taken at positions A and B, which describe the hole-like structures and the top of the flat Ni film, respectively (Figure 2g). The spectrum measured at A (Figure 2g) shows a low D-peak, sharp G-peak, and a high and sharp 2D-peak, which has a high 2D/G intensity ratio (~3). These features are consistent with those of a high-quality single-layer graphene sheet.¹⁶ There are three possibilities to realize this unique graphene growth. (1) The hole-like structures of Ni are formed before the graphene growth. (2) The hole-like structure formation and graphene growth occur together. (3) The

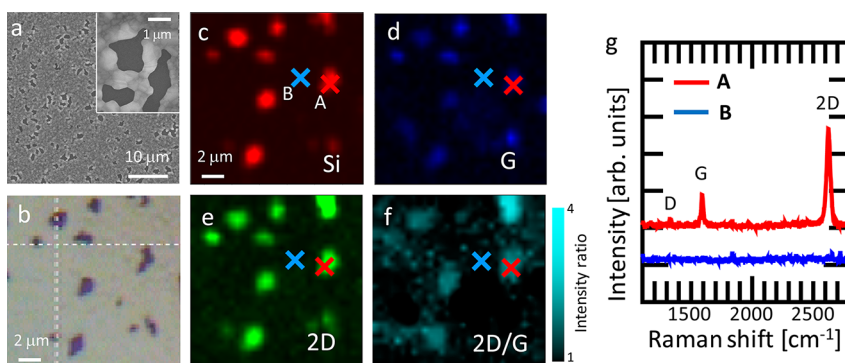


Figure 2. (a) SEM and (b) optical microscope images of the Ni surface after RH-PCVD. Inset in (a) shows a typical high magnification SEM image of hole-like structures. Integrated Raman intensity maps of the Ni surface after RH-PCVD of the (c) Si-peak, (d) G-peak, (e) 2D-peak, and (f) ratio of the 2D to G peak intensity. (g) The raw Raman scattering spectra taken at positions A and B indicated in (c).

hole-like structures are formed after the growth of graphene. Based on our systematic investigation, it was found that graphene was not grown when hole-like structures were preformed before the growth. In general, it is known that graphene growth happens during the cooling process. When we follow this model, the formation of Ni hole-like structures after the graphene growth should be difficult because the temperature of the substrate becomes low due to the cooling process. By judging from these reasons, it can be supposed that the hole-like structure formation and graphene growth happen together. The correlation with carbon concentration in Ni, substrate temperature, and melting point of Ni might be the key factors to explain the unique graphene growth. Further study is required to clarify the reason why this unique reaction happens in our system.

After removing the Ni film using a chemical etching process, interestingly, it was found that a high-quality graphene layer was also grown along the interface between the Ni film and the SiO_2 substrate. At the initial growth stage, clear hexagonal domains of graphene were observed (Figures 3a-g). The average hexagonal domain size is about $10\text{--}20\ \mu\text{m}$. Although hexagonal domain growth of graphene has been reported by several groups in recently, the growth was limited only on the metal substrates.^{17–19} This is the first result realizing the hexagonal domain growth of graphene directly on the SiO_2 substrate. This hexagonal domain growth indicates the quality of graphene grown with our established method should be relatively high, which is consistent with the low D-peak Raman scattering spectrum shown in Figure 2g. By adjusting the growth conditions, the centimeter-order large scale graphene layer was also uniformly grown on the SiO_2 substrate (Figures 3h-m), which was confirmed by optical microscopy (Figure 3h), SEM (Figure 3i), integrated Raman intensity mapping of the 2D/G intensity ratio (Figure 3j), atomic force microscopy (AFM) (Figure 3k), transmission electron microscopy (TEM) (Figure 3l), and raw Raman scattering spectra randomly taken at the same area shown in

Figure 3j (Figure 3m). The continuous dark lines were observed with $0.34\ \text{nm}$ space each by TEM observation (Figure 3l). This indicates that the structure of graphene grown by our method is not the stack of the small islands but the continuous one or a few layer sheets.

The lower limit of growth temperature was also investigated. Figures 4 show typical Raman scattering spectra as a function of growth temperature (Figure 4a) and 2D/G ratio plot for the different growth temperature (Figure 4b). Although D-peak intensity increases with a decrease in growth temperature, clear 2D band can be still observed even at $600\ ^\circ\text{C}$. This indicates that the growth temperature of graphene directly on the SiO_2 can be lowered below $600\ ^\circ\text{C}$ with RH-PCVD, which is much lower than the temperature needed for thermal CVD ($900\text{--}1000\ ^\circ\text{C}$) graphene growth.^{8–11,15} The 2D peak position and shape gradually up shifts and broadens, respectively, with a decrease in the growth temperature. Since 2D peak is known to be very sensitive to the layer number of graphene,¹⁶ this peak change indicates that the layer number of graphene might slightly increase with a decrease in growth temperature. This low direct growth temperature of graphene should be very important for the promotion of practical graphene application in electrical device fields.

To address the mechanism of the growth of graphene along the interface between the Ni and SiO_2 layers, the time evolution of the graphene growth was systematically investigated as a function of initial thickness of the Ni layer, T_{Ni} (Figure S1). When T_{Ni} was small (e.g., 25 nm), the Ni film was easily evaporated and formed nano islands. On the other hand, if the Ni film was relatively thick (e.g. $T_{\text{Ni}} = 85\ \text{nm}$) the growth between the Ni and SiO_2 layers was initiated after a long period of RH-PCVD (e.g., 20 min). At a suitable thickness ($T_{\text{Ni}} = 55\ \text{nm}$), hole-like structures were formed after a relatively short growth time ($\sim 3\ \text{min}$) and graphene was selectively grown at the interface between the Ni and SiO_2 layers. When the growth time was longer than 5 min, growth occurs on the top layer

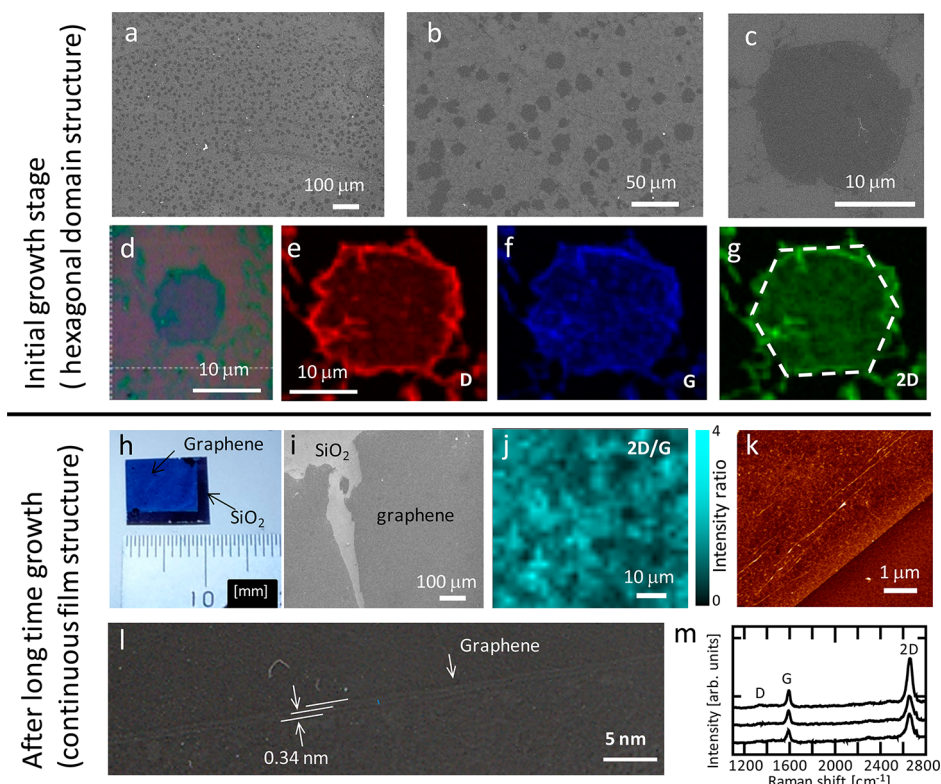


Figure 3. (a-g) Hexagonal domain of graphene directly grown on the SiO₂ substrate. (a) Low, (b) middle, and (c) high magnification SEM images of graphene with hexagonal domain structures. (d) An optical microscope and integrated Raman intensity maps of (e) D-peak, (f) G-peak, (g) 2D-peak of hexagonal domain graphene. (h-m) Uniform graphene in large scale directly grown on the SiO₂ substrate. (h) An optical image, (i) a SEM image, (j) an integrated Raman intensity map of the ratio of the 2D/G peak intensity, (k) an AFM image, (l) a TEM image, and (m) typical raw Raman scattering spectra of graphene directly grown on the SiO₂ substrate in large scale.

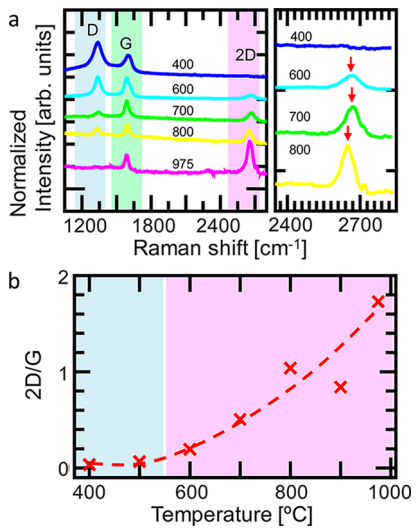


Figure 4. (a) Typical raw Raman scattering spectra of graphene at different growth temperatures. (b) 2D/G intensity ratio plot as a function of growth temperature.

and at the interface between the layers, and the initial Ni film was converted to nano islands after a growth period of 20 min, which was similar to the thin Ni layer case (25 nm) where the Ni nano islands could not be removed even after the chemical etching because the graphitic layers covered the Ni nano islands.

From these experimental results, it is conjectured that the correlation of the evaporation rate of the Ni film (E_{Ni}), the thickness of the film (T_{Ni}), and the diffusion kinetics of the carbon atoms in the Ni film should be important factors for the selective growth of graphene at the interface between the Ni and SiO₂ layers. The following three conditions should be satisfied to realize the selective growth of graphene at the Ni and SiO₂ interface. Here, we describe the carbon density in the Ni film at a distance x from the top of the Ni surface after a growth time t is $C(x,t)$. The Ni surface is always $x = 0$ during the growth. First, the Ni film structure must be maintained during the growth process, i.e., $T_{Ni} \gg E_{Ni}t$, where t denotes the growth time. Second, the carbon density at the interface between the Ni and SiO₂ layers ($x = l$) after the growth, $C(l,t)$, must be higher than the threshold density to form graphene, C_{th} , i.e., $C(l,t) > C_{th}$, $l = T_{Ni} - E_{Ni}t$. Third, the carbon density on the surface of the Ni layer ($x = 0$) after the growth, $C(0,t)$, must be lower than C_{th} , i.e., $C(0,t) < C_{th}$. The first condition can be satisfied by adjusting the initial Ni film thickness and the growth time as shown in Figure S1. $C(x,t)$ is given by solving the one-dimensional diffusion equation $(\partial C(x,t)/\partial t = D\nabla^2 C(x,t))$. This solution is $C(x,t) \propto (1/(4\pi Dt))^{1/2} \exp(-x^2/4Dt)$, where D is a diffusion coefficient.²⁰ At a specific growth time t_1 , $C(0,t_1) \propto (1/(4\pi Dt_1))^{1/2}$ and

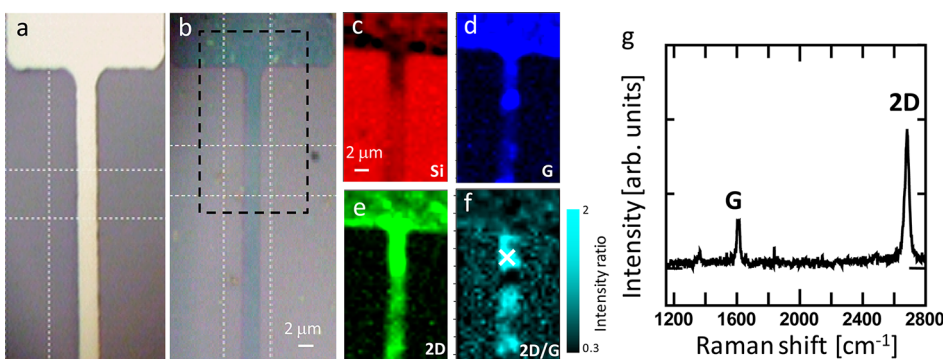


Figure 5. Optical microscope images (a) before and (b) after the growth ($950\text{ }^{\circ}\text{C}$) of graphene on the SiO_2 substrate. (c–f) Integrated Raman intensity map of the (c) Si-peak, (d) G-peak, (e) 2D-peak, and (f) ratio of the 2D to G-peak intensities of patterned graphene. The mapping area is indicated by a dotted line in (b). (g) Typical raw Raman scattering spectrum of patterned graphene taken at the position \times in (f).

$C(l,t_1) \propto (1/(4\pi Dt_1))^{1/2} \exp(-l^2/4Dt_1)$, thus $C(0,t_1) > C(l,t_1)$. This indicates that the carbon density on the top of the Ni film is always higher than that at the interface between the Ni and SiO_2 layers, and therefore it is impossible to satisfy the second and third conditions at the same time. In this model, however, it is assumed that the diffusion of carbons starts from $x = 0$, i.e., the top of the Ni layer, where the hydrocarbon materials are supplied. This is not accurate for plasma CVD. Plasma involves a large variety of high-energy hydrocarbon ions attacking the Ni surface, and some of these are high enough in energy to penetrate the surface of the Ni film to a certain depth. The penetration of high-energy ions into a solid phase is well-known phenomena as an ion implantation in current Si-based industrial fields.²¹ Thus, the position of the highest carbon density in the Ni film is not on the surface but inside the Ni layer. In this case, the diffusion starts from not $x = 0$ but $x = l_c$, where l_c is the depth to which hydrocarbons penetrate the Ni surface. If $l_c \gg T_{\text{Ni}}/2$, $C(l,t)$ approaches C_{th} faster than $C(0,t)$ and graphene can be preferentially grown only along the interface between the Ni and SiO_2 layers (Figure S2). It should be mentioned that what we want to focus on in this model is the growth site (top layer of Ni or interlayer between Ni and SiO_2) of graphene. On the basis of the systematic investigations, it was found that the growth site of graphene was mainly decided not by the temperature but by the type of CVD (thermal or plasma); that is, selective interlayer growth cannot be realized in any temperature range when we use thermal CVD in our system, and selective interlayer growth happened only when plasma was generated during the growth. Thus, we do not consider the effects of temperature in this model for simplification. For the construction of further accurate growth models of graphene, it is necessary to consider the effects of temperature on the growth of graphene.

Another effect of plasma should be a decrease of the Ni layer evaporation rate, E_{Ni} . We also attempted to grow graphene with the same experimental setup

except that we used thermal CVD instead of RH-PCVD. However, the Ni film was rapidly evaporated even if the Ni film was 55 nm thick, and graphene growth was not realized (Figure S3). Because the melting temperature of the Ni–C material increases with an increase in the concentration of C,²² E_{Ni} should also depend on the hydrocarbon flux supplied to the Ni, i.e., Γ_c . In particular, the Ni evaporation rate should decrease with an increase in the supplied hydrocarbon flux. In the case of thermal CVD, Γ_c is mainly dictated by the hydrocarbon gas pressure, whereas Γ_c in plasma CVD should be much higher due to the decomposition of source gases resulting from impacts with the energetic electrons in the plasma. The minimum Ni layer thickness, T_{Nimin} , which satisfies the first condition, is thinner when using plasma CVD than thermal CVD. This thinner Ni structure also allows the second condition to be satisfied. We also used a Cu catalyst instead of Ni in the RH-PCVD experiment. However, the Cu film was completely transformed to nanoislands, and graphene growth was not realized (Figure S4). This may be due to the lower melting point of Cu compared with that of Ni, or it may be due to a difference in the diffusion kinetics of Cu and Ni.²³

By applying this unique growth technique, the growth of patterned graphene is also possible by forming Ni patterns with a conventional photolithography technique prior to RH-PCVD. Figure 5a and b show optical microscope images of the patterned Ni film before RH-PCVD and graphene after RH-PCVD followed by chemical etching to remove the Ni film, respectively. Figure 5c–f show the integrated Raman intensity mapping of the Si-, G-, and 2D-peaks and the 2D- to G-peak intensity ratio of directly grown graphene on the SiO_2 substrate. Ribbon-like high-quality graphene (width $\sim 2\text{ }\mu\text{m}$) is selectively grown on the SiO_2 substrate, which is also confirmed by the raw Raman scattering spectrum (Figure 5g). It is worthwhile to mention that the 2D/G intensity ratio is almost constant at a relatively high value of ~ 1.8 , and the D-peak intensity is very low over the entire patterned

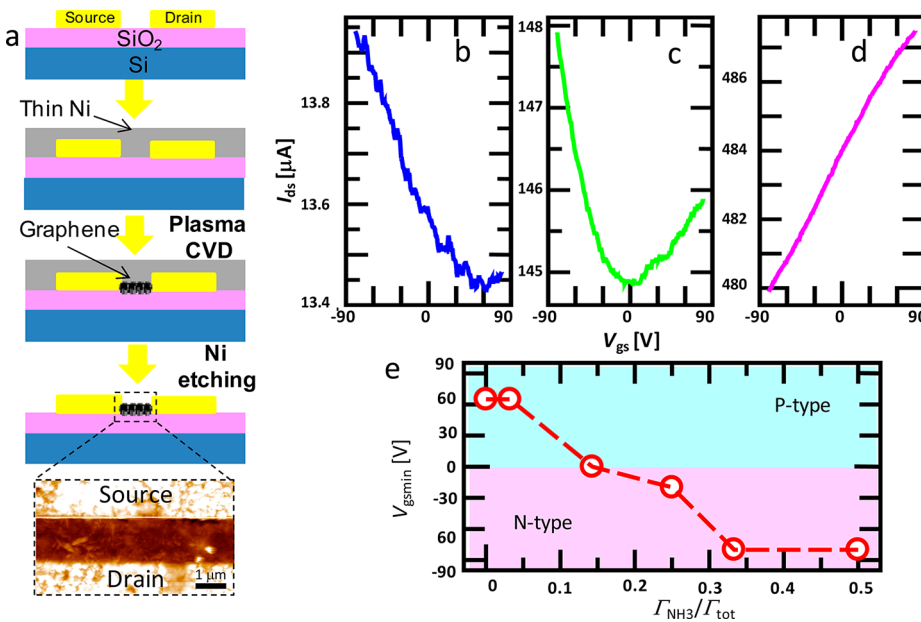


Figure 6. (a) Schematic illustration of the simple fabrication process of a graphene-based FET. (b–d) Typical I_{ds} – V_{gs} curves of graphene grown by RH-PCVD ($V_{ds} = 100$ mV) at 950 °C with NH₃ flow rates of (b) 0 sccm, (c) 5 sccm, and (d) 15 sccm. (e) V_{gsmin} – $\Gamma_{NH_3}/\Gamma_{tot}$ plot for the graphene-based FET fabricated with our direct growth method.

area, which indicates that a single layer of patterned and high-quality graphene is realized using this method. A uniform structure of single-layer and high-quality graphene is also obtained even with relatively wide ribbon structures, e.g., width $\sim 20 \mu\text{m}$ (Figure S5).

FET devices can also be fabricated using RH-PCVD. Pairs of source and drain electrodes made by Au were formed on the SiO₂ substrate. The channel length and width are ~ 1.5 and $50 \mu\text{m}$, respectively. The Ni film was then deposited on the entire substrate, and RH-PCVD was performed followed by chemical etching to remove the Ni layer. Directly grown graphene between the source and drain electrodes plays a role in the conduction channel of the FET (Figure 6a). The source–drain current, I_{ds} , was measured as a function of gate bias voltage, V_{gs} , for this FET device fabricated using the direct growth method (source–drain voltage (V_{ds}) was fixed at 0.1 V). The charge neutral point was observed at a gate bias voltage of 60 V (Figure 6b). This high gate bias voltage at the charge neutral point is due to p-doping, which is a result of the strong interaction between the SiO₂ substrate and the graphene layer grown directly on top of the substrate. This is consistent with previously reported results.¹⁵ It is known that nitrogen atoms and some nitrogen-containing compounds can be used to dope graphene with electrons.^{24–26} We therefore mixed NH₃ (diluted in Ar gas to a concentration of 10%) during the direct growth of graphene to realize the doping of the electron donor materials. Figure 6c and d show typical I_{ds} – V_{gs} curves of the graphene-based FETs fabricated with the direct growth method and various NH₃ gas flow rates. The charge neutral points are systematically shifted toward negative gate bias voltages as the NH₃

flow rate is increased, and the gate voltage can no longer be measured (*i.e.*, it is less than -80 V) with a gas flow rate of 15 sccm NH₃ (Figure 6d). The gate bias voltage at the charge neutral point (V_{gsmin}) is plotted as a function of the flow rate ratio of NH₃ to total flow ($\Gamma_{NH_3}/\Gamma_{tot}$) in Figure 6e. V_{gsmin} displays a linear dependence on the ratio $\Gamma_{NH_3}/\Gamma_{tot}$ and becomes more negative with increasing $\Gamma_{NH_3}/\Gamma_{tot}$. This indicates that it is possible to tune the concentration of the electron donor material using our direct growth method for fabricating graphene sheets on a SiO₂ substrate. This is the first time the direct growth of graphene on a SiO₂ substrate with a controllable carrier doping has been achieved. The doping density, n , can be estimated from the shift of V_{gsmin} . The gate bias voltage induces a surface charge density of $n = \epsilon_0 \epsilon |V_{gsmin}| / Te$.¹ Here, ϵ_0 and ϵ are the permittivities of free space and SiO₂, respectively; e is the electron charge; and T is the thickness of our SiO₂ layer (500 nm). If V_{gsmin} is -80 V (which occurs at $\Gamma_{NH_3} = 15$ sccm), the equation yields a surface charge density of $n \approx 3.36 \times 10^{12} \text{ cm}^{-2}$. If we assume that one nitrogen atom or nitrogen-containing material donates one electron to graphene, the density ratio of the doped nitrogen-containing material to carbon atoms in the single-layer graphene (N_{solid}/C_{solid}) is approximately 8.24/10⁴. The density ratio of the NH₃ to CH₄ in the gas phase (N_{gas}/C_{gas}) during RH-PCVD can be estimated from the pressure ratio, which gives a ratio of $N_{gas}/C_{gas} \approx 1/20$. Hence, the transition efficiency of the nitrogen-containing materials from gaseous phase to solid graphene is approximately 1.6%, which may be useful for investigating the doping kinetics of nitrogen or nitrogen-containing materials to graphene. The carrier mobilities (μ) and sheet

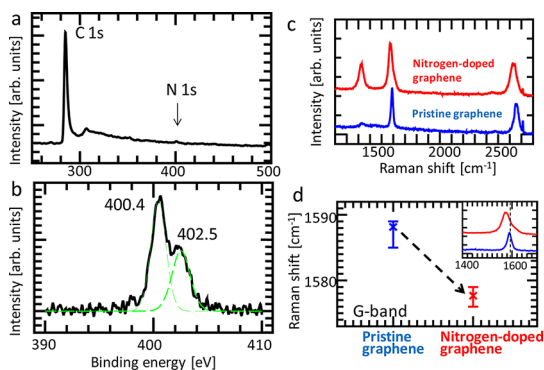


Figure 7. (a) C 1s and N 1s and (b) high-resolution N 1s XPS spectrum of nitrogen-doped graphene directly grown (950°C) on the SiO_2 substrate with $\Gamma_{\text{NH}_3}/\Gamma_{\text{tot}} = 0.5$. (c) Typical Raman scattering spectra and (d) G-peak position plot of pristine and nitrogen-doped graphene, respectively. Inset in (d) shows the typical raw G-peak spectra of pristine and nitrogen-doped graphene.

resistivities (R_s) in graphene were estimated from FET characteristics as $\mu = \sigma/en$ and $R_s = (V_{ds}/I_{ds})(W/L)$, where σ , n , W , and L denote conductivity of graphene, surface charge density induced by V_{gs} , width, and length of the graphene sheet, respectively.¹ We obtained the values of μ and R_s , which varied from sample to sample in the ranges $43\text{--}580\text{ cm}^2/(\text{V s})$ and $20\text{--}50\text{ k}\Omega/\text{sq}$, respectively. This estimated values of μ and R_s are almost on the same order and about 10 times higher, respectively, than those of graphene directly fabricated on the SiO_2 substrate by thermal CVD.¹⁵ These moderate μ and slightly higher R_s might be due to the effects of remaining Ni particles strongly coupled with graphene, which can be solved by adjusting the Ni etching process conditions. The poor contact between electrode and graphene in our device and strong coupling between graphene and the SiO_2 substrate might also be other possible reasons for the moderate μ and slightly higher R_s . Improvement of these device performances should be one of the future goals of this study.

To investigate the content of nitrogen atoms, core-level X-ray photoelectron spectroscopy (XPS) was also performed on the nitrogen-doped graphene fabricated under the condition of $\Gamma_{\text{NH}_3}/\Gamma_{\text{tot}} = 0.5$. The peaks at 284.5 and 400 eV correspond to the C 1s peak of sp^2 carbon and N 1s peak of the doped nitrogen, respectively (Figure 7a). In the high-resolution scan, the asymmetric N 1s peak can be observed as shown in

Figure 7b. This peak can be divided into two components, indicating that nitrogen atoms are in two different binding states inserted into the graphene network. On deconvolution, we found peaks at 400.4 and 402.5 eV (green curves in Figure 7b), the first one being characteristic of pyrrolic nitrogen and the second due to nitrogen in the graphene sheets.²⁷ In general, there is another peak from N 1s at 398.9 eV , which is known from pyridinic nitrogen. In our nitrogen-doped graphene, only peaks from pyrrolic nitrogen and nitrogen in the graphene were observed, which differs from the previous report of nitrogen-doped graphene by thermal CVD.²⁸ This indicates unique doping states of nitrogen might be realized by this RH-PCVD method. The atomic concentration ratio of nitrogen to carbon ($N_{\text{solid}}/C_{\text{solid}}$) can be estimated from the XPS spectra; $N_{\text{solid}}/C_{\text{solid}} = 7.8/10^4$, which is well matched with the calculated value from electrical data mentioned above ($N_{\text{solid}}/C_{\text{solid}} = 8.24/10^4$). This implies that the nitrogen atoms doped into graphene act as electron donors with relatively high charge transfer efficiency. Raman scattering spectra were also measured for nitrogen-doped graphene. As shown in Figure 7c and d, the D-peak intensity increases and the G-peak position downshifts by doping with nitrogen, which are consistent with the previous reports.^{24–26} This also supports that our established direct growth methods can realize nitrogen doping of graphene.

CONCLUSIONS

We have realized and demonstrated an easy and scalable method for the growth of high-quality graphene directly on a SiO_2 substrate that enables a precise tuning of the graphene carrier concentration. Through systematic investigations, we have shown that a relatively thin Ni layer and the RH-PCVD process are critical for the selective growth of graphene along the interface between a Ni film and the SiO_2 substrate. Easy and scalable patterning and FET fabrication processes using this direct growth method are also demonstrated. To fabricate an FET, high-quality graphene is selectively grown between the source and drain electrodes and directly on the SiO_2 substrate. The transport type of the graphene-based FET fabricated with our direct growth method can be controlled by tuning the NH_3 gas concentration during RH-PCVD.

EXPERIMENTAL METHODS

Graphene Growth by RH-PCVD. A homemade plasma CVD system was used to grow single-layer graphene. Inductively coupled plasmas were generated by supplying a radio frequency signal of 13.56 MHz to the coils, which were positioned outside a quartz tube. An electrical furnace was heated to the desired temperature prior to moving the substrate from outside the quartz tube into its center. A 9:1 mixture of methane and hydrogen gas was blown over the

area after the substrate reached the desired temperature, after which the rf power was switched on to generate the plasma. After the desired growth time, the rf power supply was switched off and the substrate was cooled rapidly by ambient room temperature.

Raman Mapping Measurements. Raman scattering spectroscopy (J/Y) with He–Ne laser excitation (632.8 nm wavelength) was used to identify the quality of the fabricated graphene. Raman mapping measurements were performed by moving the substrate holder in $200\text{--}2000\text{ nm}$ steps.

TEM Observation. The structure of graphene was also measured by a high-resolution TEM (Hitachi HF-2000) with an acceleration voltage of 200 keV.

FET Measurement. The electrical transport properties of graphene were measured using a vacuum probe station with a semiconductor parameter analyzer (HP 4511C). The base pressure was less than 10^{-4} Pa. To evaporate the adsorbed molecules such as oxygen and water, an electrical annealing process was performed on all of the devices prior to any measurements.²⁹

Conflict of Interest: The authors declare no competing financial interest.

Supporting Information Available: Time evolution of graphene growth as a function of the initial Ni film thickness. Model for graphene growth along the interface of the Ni and SiO₂ substrate layers. Comparison of the CVD methods (thermal CVD and plasma CVD) and catalysts (Ni and Cu) for the growth of graphene along the interface of the Ni and SiO₂ substrate layers. The growth of a patterned graphene ribbon over a relatively wide area. This material is available free of charge via the Internet at <http://pubs.acs.org>.

Acknowledgment. This work was supported by JSPS KAKENHI (23740405, 21654084). We are grateful to Prof. K. Tohji and Mr. K. Motomiya for their help in conducting the TEM observations.

REFERENCES AND NOTES

- Novoselov, K. S.; Geim, A. K.; Morozov, S. V.; Jiang, D.; Zhang, Y.; Dubonos, S. V.; Grigorieva, I. V.; Firsov, A. A. Electric Field Effect in Atomically Thin Carbon Films. *Science* **2004**, *306*, 666–669.
- Zhang, Y.; Tan, Y.-W.; Stormer, H. L.; Kim, P. Experimental Observation of the Quantum Hall Effect and Berry's Phase in Graphene. *Nature* **2005**, *438*, 201–204.
- Novoselov, K. S.; Jiang, Z.; Zhang, Y.; Morozov, S. V.; Stormer, H. L.; Zeitzer, U.; Maan, J. C.; Boebinger, G. S.; Kim, P.; Geim, A. K. Room-Temperature Quantum Hall Effect in Graphene. *Science* **2007**, *315*, 1379.
- Lin, Y.-M.; Dimitrakopoulos, C.; Jenkins, K. A.; Farmer, D. B.; Chiu, H.-Y.; Grill, A.; Avouris, Ph. 100-GHz Transistors from Wafer-Scale Epitaxial Graphene. *Science* **2010**, *327*, 662.
- Liu, Z.; Liu, Q.; Huang, Y.; Ma, Y.; Yin, S.; Zhang, X.; Sun, W.; Chen, Y. Organic Photovoltaic Devices Based on a Novel Acceptor Material: Graphene. *Adv. Mater.* **2008**, *20*, 3924–3930.
- Schedin, F.; Geim, A. K.; Morozov, S. V.; Hill, E. W.; Blake, P.; Katsnelson, M. I.; Novoselov, K. S. Detection of Individual Gas Molecules Adsorbed on Graphene. *Nat. Mater.* **2007**, *6*, 652–655.
- Dong, X.; Shi, Y.; Huang, W.; Chen, P.; Li, L.-J. Electrical Detection of DNA Hybridization with Single-Base Specificity Using Transistors Based on CVD-Grown Graphene Sheets. *Adv. Mater.* **2010**, *22*, 1649–1653.
- Reina, A.; Jia, X.; Ho, J.; Nezich, D.; Son, H.; Bulovic, V.; Dresselhaus, M. S.; Kong, J. Large Area, Few-Layer Graphene Films on Arbitrary Substrates by Chemical Vapor Deposition. *Nano Lett.* **2009**, *9*, 30–35.
- Kim, K. S.; Zhao, Y.; Jang, H.; Lee, S. Y.; Kim, J. M.; Kim, K. S.; Ahn, J.-H.; Kim, P.; Choi, J.-Y.; Hong, B. H. Large-Scale Pattern Growth of Graphene Films for Stretchable Transparent Electrodes. *Nature* **2009**, *457*, 706–710.
- Li, X.; Cai, W.; An, J.; Kim, S.; Nah, J.; Yang, D.; Piner, R.; Velamakanni, A.; Jung, I.; Tutuc, E.; et al. Large-Area Synthesis of High-Quality and Uniform Graphene Films on Copper Foils. *Science* **2009**, *324*, 1312–1314.
- Ago, H.; Ito, Y.; Mizuta, N.; Yoshida, K.; Hu, B.; Orofeo, C. M.; Tsuji, M.; Ikeda, K.; Mizuno, S. Epitaxial Chemical Vapor Deposition Growth of Single-Layer Graphene over Cobalt Film Crystallized on Sapphire. *ACS Nano* **2010**, *4*, 7407–7414.
- Li, X.; Wang, X.; Zhang, L.; Lee, S.; Dai, H. Chemically Derived, Ultrasmooth Graphene Nanoribbon Semiconductors. *Science* **2008**, *319*, 1229–1232.
- Zhang, L.; Shi, Z.; Wang, Y.; Yang, R.; Shi, D.; Zhang, G. Catalyst-Free Growth of Nanographene Films on Various Substrates. *Nano Res.* **2011**, *4*, 315–321.
- Ismach, A.; Druzgalski, C.; Penwell, S.; Schwartzberg, A.; Zheng, M.; Javey, A.; Bokor, J.; Zhang, Y. Direct Chemical Vapor Deposition of Graphene on Dielectric Surfaces. *Nano Lett.* **2010**, *10*, 1542–1548.
- Su, C.-Y.; Lu, A.-Y.; Wu, C.-Y.; Li, Y.-T.; Liu, K.-K.; Zhang, W.; Lin, S.-Y.; Juang, Z.-Y.; Zhong, Y.-L.; Chen, F.-R.; et al. Direct Formation of Wafer Scale Graphene Thin Layers on Insulating Substrates by Chemical Vapor Deposition. *Nano Lett.* **2011**, *11*, 3612–3616.
- Dresselhaus, M. S.; Jorio, A.; Hofmann, M.; Dresselhaus, G.; Saito, R. Perspectives on Carbon Nanotubes and Graphene Raman Spectroscopy. *Nano Lett.* **2010**, *10*, 751–758.
- Wu, B.; Geng, D.; Guo, Y.; Huang, L.; Xue, Y.; Zheng, J.; Chen, J.; Yu, G.; Liu, Y.; Jiang, L.; et al. Equiangular Hexagon-Shape-Controlled Synthesis of Graphene on Copper Surface. *Adv. Mater.* **2011**, *23*, 3522–3525.
- Yu, Q.; Jauregui, L. A.; Wu, W.; Colby, R.; Tian, J.; Su, Z.; Cao, H.; Liu, Z.; Pandey, D.; Wei, D.; et al. Control and Characterization of Individual Grains and Grain Boundaries in Graphene Grown by Chemical Vapour Deposition. *Nat. Mater.* **2011**, *10*, 443–449.
- Robertson, A. W.; Warner, J. H. Hexagonal Single Crystal Domains of Few-Layer Graphene on Copper Foils. *Nano Lett.* **2011**, *11*, 1182–1189.
- Fick, A. E. On Liquid Diffusion. *Philos. Mag.* **1855**, *4*, 30–39.
- Dearnaley, G. Ion Implantation. *Nature* **1975**, *256*, 701–705.
- Singleton, M.; Nash, P. The C-Ni (Carbon-Nickel) System. *J. Phase Equilib.* **1989**, *10*, 121–126.
- Li, X.; Cai, W.; Colombo, L.; Ruoff, R. S. Evolution of Graphene Growth on Ni and Cu by Carbon Isotope Labeling. *Nano Lett.* **2009**, *9*, 4268–4272.
- Wei, D.; Liu, Y.; Wang, Y.; Zhang, H.; Huang, L.; Yu, G. Synthesis of N-Doped Graphene by Chemical Vapor Deposition and Its Electrical Properties. *Nano Lett.* **2009**, *9*, 1752–1758.
- Li, X.; Wang, H.; Robinson, J. T.; Sanchez, H.; Diankov, G.; Dai, H. Simultaneous Nitrogen Doping and Reduction of Graphene Oxide. *J. Am. Chem. Soc.* **2009**, *131*, 15939–15944.
- Kato, T.; Jiao, L.; Wang, X.; Wang, H.; Li, X.; Zhang, L.; Hatakeyama, R.; Dai, H. Room-Temperature Edge Functionalization and Doping of Graphene by Mild Plasma. *Small* **2011**, *7*, 574–577.
- Casanovas, J.; Ricart, J. M.; Rubio, J.; Illas, F.; Jimenez-Mateos, J. M. Origin of the Large N 1s Binding Energy in X-ray Photoelectron Spectra of Calcined Carbonaceous Materials. *J. Am. Chem. Soc.* **1996**, *118*, 8071–8076.
- Jin, Z.; Yao, J.; Kittrell, C.; Tour, J. M. Large-Scale Growth and Characterizations of Nitrogen-Doped Monolayer Graphene Sheets. *ACS Nano* **2011**, *5*, 4112–4117.
- Wang, X.; Li, X.; Zhang, L.; Yoon, Y.; Weber, P. K.; Wang, H.; Guo, J.; Dai, H. N-Doping of Graphene Through Electro-thermal Reactions with Ammonia. *Science* **2009**, *324*, 768–771.